ACS OMEGA

Article

Cite This: ACS Omega 2018, 3, 14924−14932

http://pubs.acs.org/journal/acsodf

Development of Thick Superhydrophilic TiO_2−ZrO_2 Transparent Coatings Realized through the Inclusion of Poly(methyl methacrylate) and Pluronic-F127

Sanu M. Simon,[†] Anoop Chandran,[‡] Gejo George,[†] M. S. Sajna,[†] Prakashan Valparambil,[†] Eric Kumi-Barmiah,[§] Gin Jose,[§] P. R. Biju,[†] Cyriac Joseph,[†] and N. V. Unnikrishnan*[,†]

[†]School of Pure & Applied Physics, Mahatma Gandhi University, Kottayam 686 560, Kerala, India

[‡]Department of Physics, St. Cyril's College, Adoor 691 529, Kerala, India

[§]School of Chemical and Process Engineering, University of Leeds, Leeds LS2 9JT, U.K.

ABSTRACT: A thick coating of hierarchically porous double-templated TiO_2−ZrO_2−PMMA−PF127 with excellent self-cleaning properties and high transmittance has been developed for the first time on glass substrates using a simple dip-coating technique. Comparative studies of this sample with a thick and transparent coating of single-templated TiO_2−ZrO_2−PMMA have been performed to probe the origin of its exceptional properties. The formation of the composites, successful incorporation of the polymer into the matrix, and the porous nature of the films have been studied. The presence of Ti^{2+} in the double-templated samples has been confirmed, which suggest the chemisorption of water on the surface of the film. The variation in the self-cleaning properties of the samples on UV-illumination has also been studied. The double-templated film is found to possess the capability of good hydrophilic retention even 2 days after UV-irradiation.

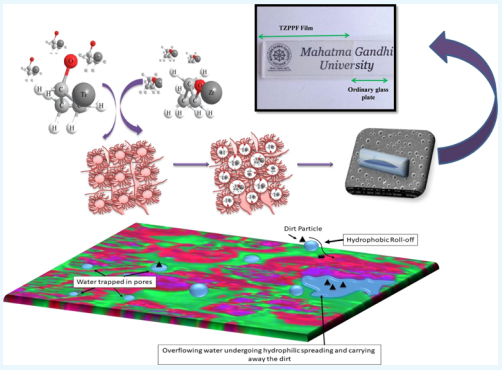

INTRODUCTION

It has been reported that hydrophilic coatings of inorganic metal oxides with large surface area and high porosity clean the surface quickly.[1] Addition of polymers to inorganic binary metal oxide composites, on the other hand, is known to facilitate the spreading nature of liquid, and the surface roughness can trap the water molecules.[2] Theoretical works of Wenzel and Cassie−Baxter suggest that maximal increase in wetting property of the surface can be achieved by the enhancement of its roughness.[3−5] Also, there are many recent reports on hydrophilicity achieved through nanoporous structure formation on the film surface.[2,6] Therefore, multifunctional polymer-incorporated inorganic composites in the form of meso/micro/macroporous films, membranes, and powders are of great significance as they have potential applications as self-cleaning glasses for solar cells, gas-sensing devices, photovoltaic devices, and window glass for green intelligent buildings.[7−11]

TiO_2 as a self-cleaning coating has high transmittance and has the advantage to make use of both solar energy and rainfall to clean the surface, which reduces the cost of maintenance.[12] For further improving the transmittance, hydrophilicity, and mechanical and thermal stabilities, the general approach is to synthesize binary composites involving TiO_2 and a low refractive index material such as ZrO_2, SiO_2, and so forth.[13] The excess amount of hydroxyl groups present in TiO_2−ZrO_2/TiO_2−SiO_2 hybrid composites trap photoinduced holes, which increase the photocatalytic activity by delaying the recombination of electron−hole pairs.[14] This implies that such a coating would be able to breakdown the dirt absorbed onto its surface in the presence of sunlight.[15]

The hydroxyl group-trapping ability of TiO_2−ZrO_2/SiO_2 along with high porosity of polymer-incorporated composites can be combined together in TiO_2−ZrO_2/SiO_2−polymer coatings. Although there are a few reports on the hydrophilic nature of such coatings, some major disadvantages of such films remain unaddressed.[16,17] The development of such coatings is of extreme significance, and efforts are underway to realize them. In most of the literature, which reports the formation of superhydrophilic transparent coatings, the thickness of the coating is on the nanoscale.[12,14,17] Nevertheless, the large-scale production of such thin self-cleaning glasses is really expensive because of the sophisticated techniques involved. In this work, single-templated and double-templated porous, thick, yet transparent films of TiO_2−ZrO_2−pluronic F127 (PF127), and/or poly(methyl methacrylate) (PMMA) have been prepared via the sol-gel dip-coating method. The prepared samples are found to exhibit excellent self-cleaning properties, which can be substantially retained for hours. Such coatings have significant scientific and

Received: August 8, 2018
Accepted: October 19, 2018
Published: November 6, 2018

DOI: 10.1021/acsomega.8b01940
ACS Omega 2018, 3, 14924−14932

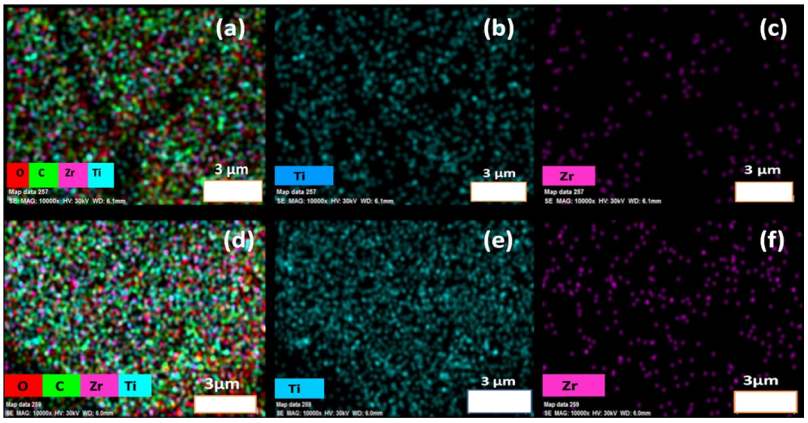

Figure 1. Elemental mapping analysis of each element present in (a–c) TZPPF film and (d–f) TZP film.

technological importance as their properties can easily be tailored by controlling the stoichiometry of the composition, type of polymer, and synthesis parameters.

RESULTS AND DISCUSSION

Structural Characterization. The composition of the as-prepared coatings is primarily analyzed using elemental mapping and Fourier transform infrared (FTIR) spectra. The elemental maps of titanium (Ti), carbon (C), oxygen (O), and zirconium (Zr) in both TZP and TZPPF are obtained using SEM and shown in Figure 1a–f. Composition of Ti is larger than that of Zr, which is obvious from the mapping and all of the elements are evenly distributed. In addition, it can also be seen that the distribution of Ti is more even in TZPPF, which may be an indicative of the importance of role played by the structure directing agent in molding the fabric of film.

The FTIR spectra (Figure 2) of the samples show a small peak at 460 cm^{-1} corresponding to the Ti–O vibrations.[18] The

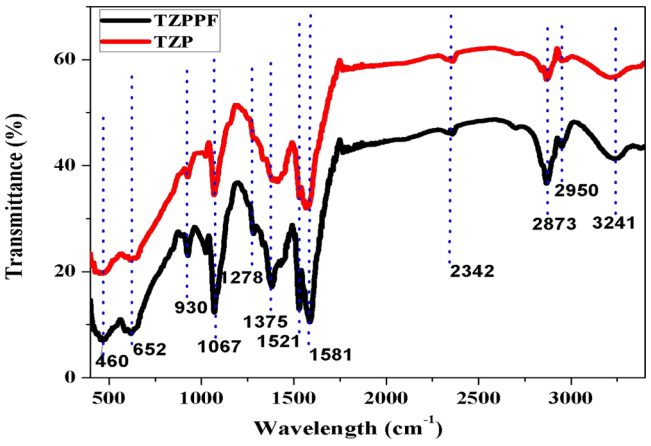

Figure 2. Comparative FTIR spectrum for the region 400–4000 cm^{-1} of the films.

low-frequency band at 930 cm^{-1} is attributed to Ti–O–Ti stretching vibrations.[19−21] The weak band observed at 652 cm^{-1} corresponds to the Zr–O–Ti bond, which authenticates the composite formation.[22] The broad band at 3241 cm^{-1} in both spectra depicts the bending vibrations of OH groups originating from the moisture adsorbed on PMMA. The C–O–C stretching vibrations arising from the copolymer PF127 also exist at 1067 cm^{-1}, which overlaps with the Ti–O bond vibrations.[21,22] The additional peak at 1375 cm^{-1} represents the presence of CH_2 and C–C bonds of PF127. The increase in the intensity of absorption is mainly seen at 1278, 2873, and 2950 cm^{-1} in TZPPF. This is due to the presence of the polymer PF127, which is absent in TZP.[23]

In order to study the structure of the film thoroughly, Raman spectroscopic studies of the films were carried out. The Raman spectra of the samples excited with 633 nm line of He–Ne laser are shown in Figure 3a,b. Using group theory, six active Raman modes $A_{1g} + 2B_{1g} + 3E_g$ are predicted for tetragonal ZrO_2 in the range 100–1000 cm^{-1}, whereas monoclinic ZrO_2 shows 18 active bands like doublet peak at 180 cm^{-1} and so forth.[22] TiO_2 mainly exists in two forms: anatase and rutile. Raman fundamental modes for anatase TiO_2 are appearing at 144 (E_g), 399 (B_{1g}), 519 (B_{1g}), and 639 cm^{-1}(E_g), respectively, whereas those of rutile occur at 143 cm^{-1} (B_{1g}), 447 cm^{-1} (E_g), 612 cm^{-1} (A_{1g}), and 826 cm^{-1} (B_{2g}).[24] It is obvious that the positions of some Raman bands of TiO_2 and ZrO_2 are in close proximity because of which it is difficult to distinguish them in the spectra. Eight peaks can be observed at 180, 433, 510, 565, 663, 824, 887, and 947 cm^{-1} for the TZPPF film, and these peaks belong to the fundamental vibrations of TiO_2 and ZrO_2. The bands at 433, 887, and 947 cm^{-1} are assigned to Ti–O vibrations, whereas those at 180, 824, and 565 cm^{-1} are ascribed to Zr–O vibrations. The peak at 510 cm^{-1} is attributed to Ti–O, which is clearly observable in the TZPPF film. For the TZP film, peaks are observed at 186, 428, 565, 663, 818, 885, and 951 cm^{-1}. The peaks at 428, 886, and 951 cm^{-1} belong to TiO_2, whereas ZrO_2 peaks are observed at 186, 818, and 565 cm^{-1}.[22,25−27] In the spectra of both films, the peak at 663 cm^{-1} is observed, which is characteristic for both anatase-TiO_2 and monoclinic-ZrO_2.[28] Thus, Raman spectra of composite films show peaks corresponding to both anatase-TiO_2 and monoclinic-ZrO_2. This implies that although the incorporation of ZrO_2 into TiO_2 leads to the mixed metal-oxide network as evident from FTIR, part of the matrix is formed of separate phases of TiO_2 and ZrO_2.[29,30]

Surface Morphology. The formation of porous structures in the as-prepared coatings is confirmed using small-angle X-ray scattering (SAXS) and wide-angle X-ray scattering (WAXS) investigations, which are shown in Figure 4a–f. From the figure, it is evident that the SAXS plot of double-templated composite TZPPF film shows peak corresponding to diffused scattering at lower 2θ values.[31] The main reason for this scattering in TZPPF is its surface roughness resulting from

DOI: 10.1021/acsomega.8b01940
ACS Omega 2018, 3, 14924–14932

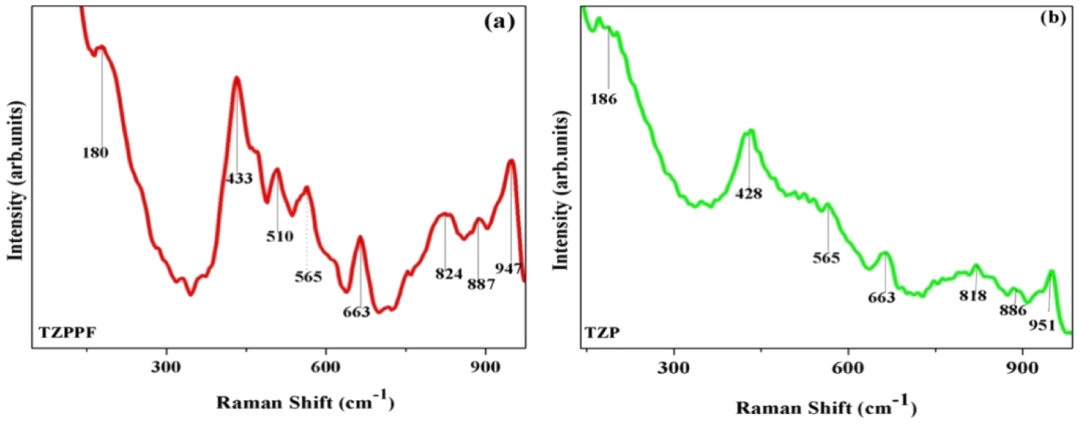

Figure 3. Raman spectra for (a) TZPPF film and (b) TZP film.

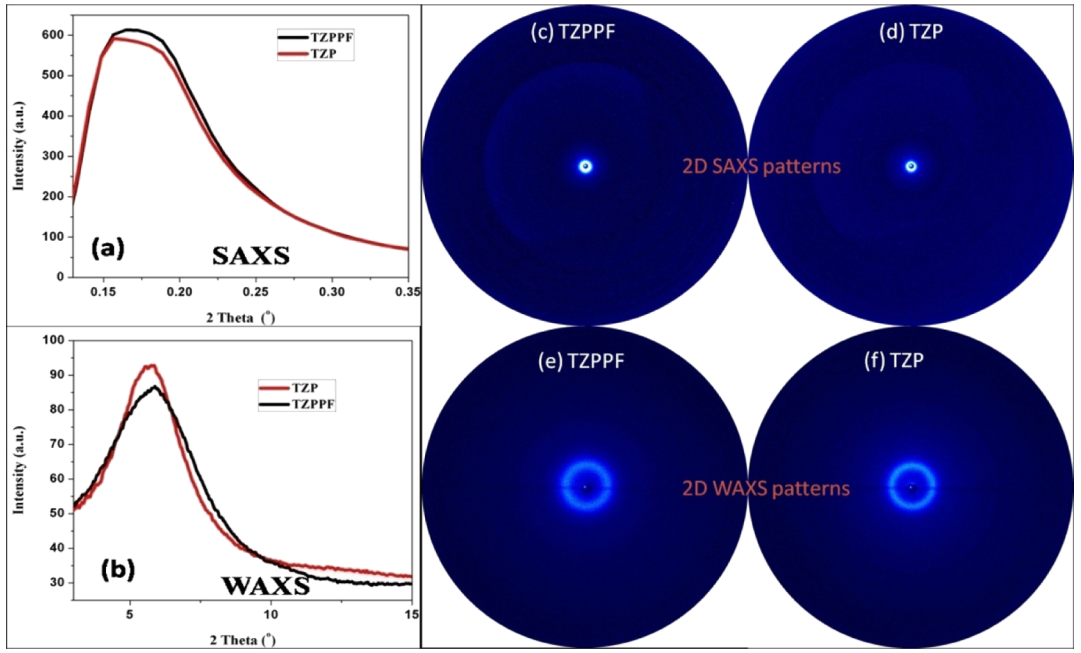

Figure 4. (a) SAXS pattern and (b) WAXS patterns of TZPPF and TZP composites. 2D SAXS pattern of (c) TZPPF and (d) TZP, and 2D WAXS pattern of (e) TZPPF and (f) TZP.

the pore formation.[32] On the contrary, in the case of TZP, a small shoulder appears in the scattering curve. This has to do with the short-range crystalline nature of the titania−zirconia matrix rather than diffused scattering. Thus, the SAXS result confirms that the composite-containing PF127 is highly porous owing to the disappearance of the shoulder at 0.18°, whereas the pores are absent in the sample with PMMA only. The faint rings in the 2D-SAXS diffraction pattern denote the presence of domains with the same structure but with different orientations corresponding to the surface. These domains are formed as a result of the mesostructure organization of pluronic F127. Such rings, however, are not observed distinctively in TZP because of the absence of domains.[33] The WAXS analysis also confirms that the porosity is present in TZPPF as the intensity of its diffraction peak at 5.6° has reduced compared to the other sample. The presence of reflections in the WAXS for both the samples highlights the absence of structural degradation of the inorganic matrix even after the addition of pluronic F127.[34,35]

A comparison of field emission scanning electron microscopy (FESEM) images (Figure 5a,b) clearly shows the formation of surface porosity in TZPPF, whereas such a nature is absent in TZP. From Figure 5a, it is clear that there are pores as large as 65 nm and as small as 10 nm and these pores are spread all over the surface. This proves that the film has a bimodal porous (mesopores and macropores) structure, and because these pores are accessible from the top, the water falling on the surface can easily diffuse through the porous framework. The thicknesses of TZP and TZPPF composite films are very close having values of 2.65 and 2.56μm, respectively, as shown in Figure 5c,d which depicts the cross-sectional view of the coatings.

Although the FESEM images clearly disclose the porosity of the sample, it gives very limited idea about the surface roughness. Therefore, atomic force microscopy (AFM) studies are performed to gather information about surface roughness. The 2D AFM images of double-templated and single-templated films are recorded and are shown in Figure 6a,b respectively. These figures are similar to the FESEM images as

DOI: 10.1021/acsomega.8b01940
ACS Omega 2018, 3, 14924−14932

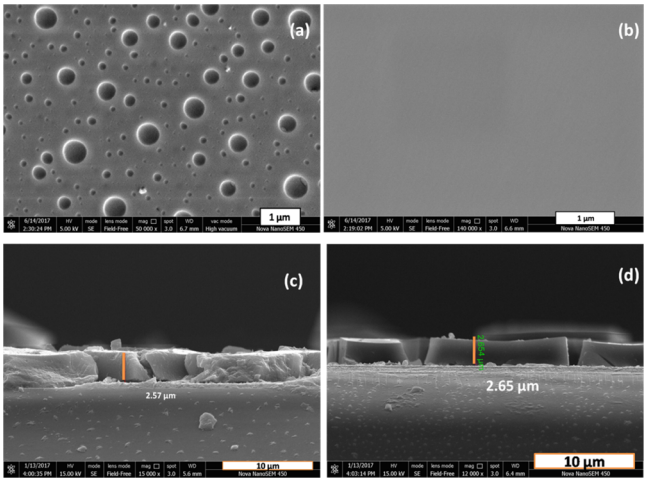

Figure 5. FESEM images of (a) TZPPF film at 1 μm and (b) TZP film at 1 μm. Lateral cross section of (c) TZP and (d) TZPPF films.

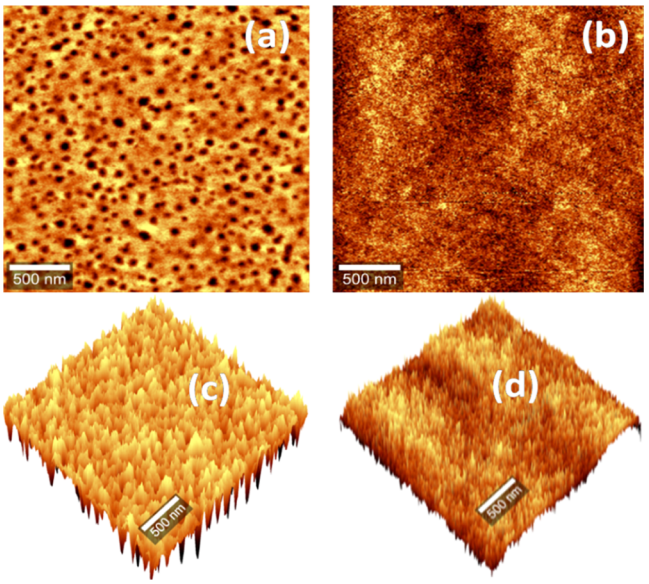

Figure 6. 2D AFM images of surface of (a) TZPPF film and (b) TZP film. 3D AFM images of surface of (c) TZPPF film and (d) TZP film.

the former shows the formation of mesoporous structure, whereas the latter has no such characteristic. The 3D AFM images shown in Figure 6c,d show regular nanotroughs and nanopits at the surface of both samples, which, however, is prominent and well distinguishable only in TZPPF. The parameters used for characterizing surface roughness are average roughness (S_a), root-mean-square roughness (S_q), skewness (S_{sk}), and kurtosis (S_{ku}). The S_a, S_q, S_{sk}, and S_{ku} values for the TZP are evaluated to be 0.473 nm, 0.595 nm, −0.032, and 3.124, respectively, whereas for TZPPF their respective values are 1.236 nm, 1.657 nm, −1.298, and 5.299. Because the TZPPF has S_q value higher than 1 nm, it can be inferred that it has a spherical pore shape with highly roughened air/solid interface. Single-templated thin film on the other hand, with a S_q value less than 1 nm, has an ultraflat surface as confirmed by the FESEM analysis.[36] Kurtosis and skewness values help to describe deviation in texture characteristics such as height distribution, surface roughness, and so forth. The negative value of skewness represents the symmetry of peaks and valleys skewed upward relative to the average surface plane as the center. The kurtosis value greater than 3 implies that surface height distribution is not Gaussian-like, which implies relatively spiky surfaces.[37,38] Comparing the skewness and kurtosis value of both surfaces, it is obvious that the TZPPF surface is more spiky with dominant peaks compared to the TZP surface. Thus, the FESEM and AFM studies together confirm the bimodal porous structure of the TZPPF film. Increase in surface roughness is also clearly demonstrated from the AFM analysis.

Although the FESEM and AFM images have shown that both mesopores and macropores are present in the surface layers of TZPPF, these studies failed to confirm the presence of micropores. For verifying if micropores are present in the samples, high-resolution transmission electron microscopy (HR-TEM) images of the surface are taken, which are shown in Figure 7. The figure shows a close-up view of the

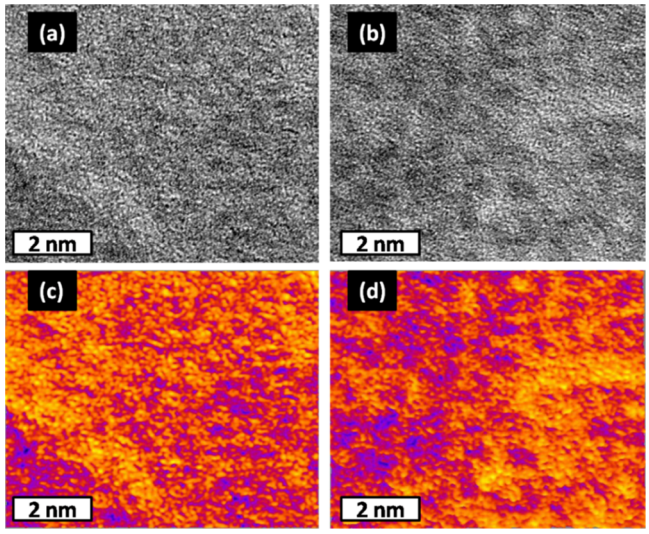

Figure 7. HR-TEM images of (a) TZP and (b) TZPPF films. Their respective color contrast versions are labeled as (c,d).

surface of both samples. The darker regions in the images indicate thicker portions on the surface. This indirectly signals the surface roughness of the film. These regions can better be distinguished using color contrast versions of the images. From Figure 7c,d it is evident that the thicker regions (blue) are scattered in TZP. It can also be seen that there exist no large patches of thinner regions (golden) in this sample. On the other hand, the thicker regions of TZPPF prevail as small clusters. These clusters are not scattered as much as they are in TZP and large patches of thinner regions are also found to exist on the surface of this film. The results give a clear indication of higher surface roughness and micropore formation in TZPPF, which makes it a trimodal porous system.

The Raman mapping images of the surface of samples are shown in Figure 8, which reveals the distribution of various components. The individual components in the composite are assigned different colors as indicated in the figure for the sake of identification. It is obvious from Figure 8a that on the surface of TZPPF coating, there are thick green lumps of polymer, which actually covers some portions of the TiO_2–ZrO_2 distribution. They are also interconnected by thin strands of polymers. On keen observation, it can be seen that these lumps of polymers create the walls of the pores. However, the floors (and in some areas the lower walls) of these pores would

DOI: 10.1021/acsomega.8b01940
ACS Omega 2018, 3, 14924−14932

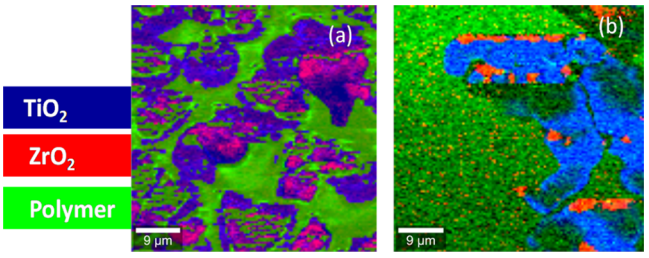

Figure 8. Raman mapping showing the distribution of elements in (a) TZPPF film and (b) TZP film. Images are plotted on the relative intensity scale. Colors other than the assigned colors arise due to the associated presence of the constituents.

mostly be built of TiO_2−ZrO_2. Contrarily, large well-distinguishable blocks of polymer and semiconductor matrix are found to exist in TZP as PF127 is absent in them. This suggests that pores are not formed in this sample, which is substantiated by the Raman mapping images.

Superhydrophilicity and Transmittance of the Films. The wetting behavior of the as-prepared films having different surface topographies has been evaluated using contact angle (CA) measurements. CA is the angle between solid surface and tangent to the liquid surface at the contact point. Parameters such as surface energy, work of adhesion, and spreading coefficient (S_c) can be calculated using CA values. A positive value of spreading coefficient indicates that a liquid will wet immediately and spread on the surface of the sample completely. Finite CA (i.e., > 0°) means S_c will be negative, which implies the lack of spontaneous wetting.[39−41]

CA measurements of TZPPF and TZP are carried out before and after UV-treatment, and the CA values and its related parameters are listed in Table 1. The untreated composite film with PF127 behaves as a better wetting surface as evidenced by its lower CA of 57° as compared to 92° of the TZP. This has directly to do with the porous structure and high roughness of the former whose joint effect would help smooth spreading and channeling of the water. This is mainly called the "wicking effect", in which the water in contact with the film surface will be drawn to the pores by capillary suction force, which later flows easily through the valleys on the surface. Furthermore, these composite surfaces have large number of hydrocarbon molecules. The force that links hydrocarbons together is much stronger than the force between water molecules, and hence water on the composite wets the surface. The possibility of polar and nonpolar interactions across the interface also gives higher adhesion between water and composite. A lower value of S_c for double-templated composite as compared to the single-templated one indicates that the former's surface is more hydrophilic.[42] This is substantiated by the observation of higher work of adhesion value for TZPPF, which suggests that larger amount of energy is required to separate water drops from its surface than that of TZP.

Further enhancement in the spreading of water is possible by treating the films with UV illumination as TiO_2 is abundant in the matrix. The water CAs (WCAs) for TZP and TZPPF thin films after 3 h of UV irradiation are found to get reduced to a great extent, acquiring the values 29° and 19°, respectively. Such an enhancement occurs because of the photogeneration of electron−hole pairs in TiO_2 during UV illumination. This will result in the reduction of Ti^{4+} cations to Ti^{3+} state and oxidation of O_2^- anions thus expelling some oxygen atoms.

X-ray photoelectron spectroscopy (XPS) studies are performed on the samples to analyze the presence of Ti^{2+} in TZPPF and hence conforming the accuracy of the proposed model, and the corresponding spectra are shown in Figure 9a,b. It is obvious that TZP samples have no pores on its surface. The Ti $2p_{3/2}$ spin−orbital splitting photoelectrons are observed near to the binding energy of 458 eV for both films. The deconvolution of the broad Ti $2p_{3/2}$ peak of the TZPPF thin film gives three components with binding energies 458.6, 458.2, and 455.1 eV, respectively. Interestingly, for TZP, the very same peak when deconvoluted gives only two components with binding energies 457.8 and 456.5 eV. The bands at 458.6 eV for TZPPF film and 457.8 eV in TZP film are assigned to Ti^{4+} $2p_{3/2}$, which confirms the formation of TiO_2.[43] Peaks occurring at binding energies 458.2 and 456.5 eV, respectively, for TZPPF and TZP indicate the Ti^{3+} $2p_{3/2}$ state, whereas the presence of an additional small shoulder at 455.09 eV in the spectra of the former sample corresponds to the Ti^{2+} $2p_{3/2}$ state.[44] It can be noted that the most intense component in the deconvoluted $2p_{3/2}$ peak for the TZPPF thin film on the higher energy part corresponds to the Ti^{4+} state, whereas the other components with second largest and smallest peaks belong to the Ti^{3+} and Ti^{2+} states, respectively.[17,44−47] The intensity ratio of the peak corresponding to Ti^{4+} to that of Ti^{3+} (i.e., $I^{Ti^{4+}}/I^{Ti^{3+}}$) for TZPPF is lower compared to that of the TZP film, which means that major portion of titanium in TZP assumes a 4+ oxidation state. Thus, the feeble presence of Ti^{3+} in TZP would be unable to endow the material with hydrophilic nature till UV-irradiation is realized in order to generate more Ti^{3+}. These Ti^{3+} would physisorb the water to the surface, which would make it hydrophilic as reported by Takeuchi et al.[48] On the other hand, Figure 9a suggests that the TZP has much reduced concentration of Ti^{4+}, which enables it to chemisorb water from the atmosphere with the aid of its pores. Such a

Table 1. Contact Angle and Its Related Parameters

Film Labels	Contact Angle [deg]	Spreading Coefficient (S_c) [mJ/m^2]	Work of Adhesion [mJ/m^2]
TZP	92.11	75.48	70.12
TZPPF	57.84	34.05	111.55
TZP (UV irradiated 3 h)	29.32	09.33	136.26
TZPPF (UV irradiated 3 h)	19.91	04.35	141.24
TZP (UV irradiated 6 h)	25.27	06.96	138.63
TZPPF (UV irradiated 6 h)	10.09	01.28	144.12
TZP (24 h after 6 h UV irradiation)	32.73	11.89	133.70
TZPPF (24 h after 6 h UV irradiation)	11.03	01.14	144.45
TZP (48 h after 6 h UV irradiation)	53.80	29.80	115.79
TZPPF (48 h after 6 h UV irradiation)	17.60	3.44	142.15

DOI: 10.1021/acsomega.8b01940
ACS Omega 2018, 3, 14924−14932

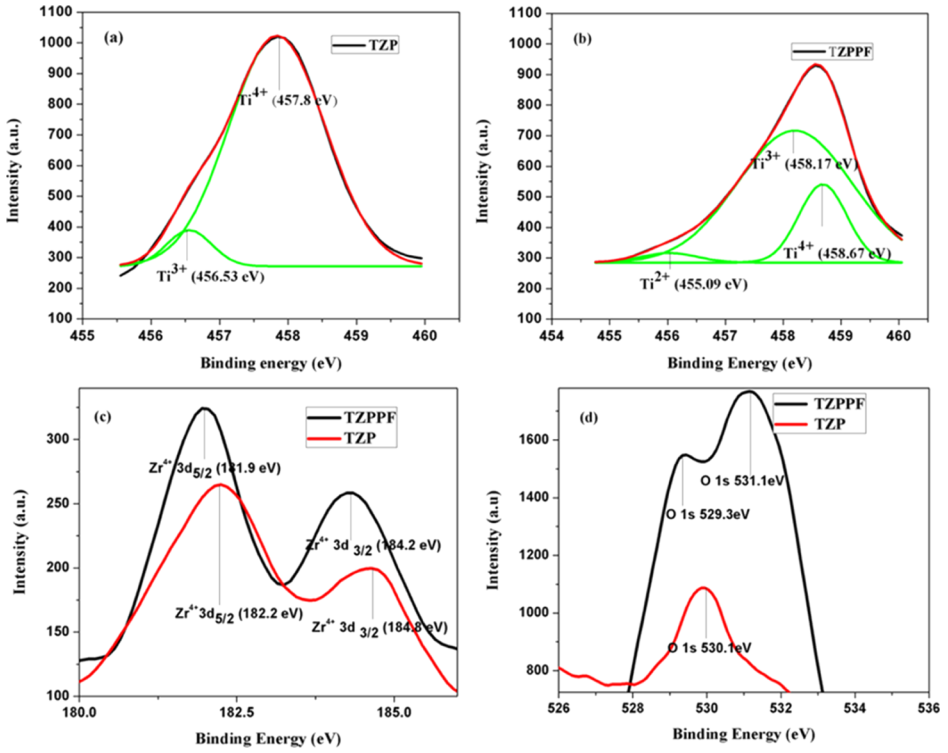

Figure 9. XPS spectra of Ti $2p_{3/2}$ in (a) TZP and (b) TZPPF films, (c) Zr 3d, and (d) O 1s.

reduction in Ti^{4+} concentration is a result of the higher surface area of the porous film, which exposes more titanium atoms to the surrounding as backed by the Raman imaging and HR-TEM studies discussed earlier. The most interesting observation that is made from the XPS is the strong presence of Ti^{2+} in TZPPF. Such an intense peak gives a strong indication of the formation of hydrogen bonding as a result of chemisorption of water. It can be noted that Ti^{2+} is absent in TZP, which is a consequence of the absence of pores in it.

Further evidence of the Ti^{2+} oxidation state in the sample can be obtained from the XPS peaks corresponding to oxygen, which are shown in Figure 9d. The O 1s spectrum for TZPPF can be observed to be broad with the main peak at 531.1 eV and a shoulder at 529.3 eV. The peak at 531.1 eV is assigned to the elemental O 1s, which makes bonds with Ti^{4+} and Ti^{3+}. The shoulder observed at 529.3 eV in the XPS of TZPPF is attributed to the presence of oxygen, bonded with Ti^{2+} in the sample.[49] The lower binding energy in this case, which finds its origin in the chemisorption of water, is understandable because the binding energy of typical covalent bond, which exists in titania, is much higher. It can be observed that for TZP, no such peak is observed, which suggests that no chemisorption is occurring in the sample. A similar result would not be observed in the case of zirconia because it is not hydrophilic all by itself. The Zr 3d XPS spectra have two peaks corresponding to Zr $3d_{5/2}$ and Zr $3d_{3/2}$ and are shown in Figure 9c. The Zr^{4+} $3d_{5/2}$ spin−orbital splitting levels for TZP and TZPPF are located at binding energies of 182.2 and 181.9 eV, respectively, whereas their corresponding binding energies of Zr^{4+} $3d_{3/2}$ level are 184.2 and 184.8 eV, respectively.[14,46]

It can be observed from Table 1 that on increasing the UV-irradiation time to 6 h, the CA is found to further diminish to about 25° and 10° for TZP and TZPPF, respectively, which suggests that the latter attains the superhydrophilic nature. It is worth noting that when the illumination time is increased, the CA decreases only by 4° in the case of TZP, whereas a reduction of 9° is observed in TZPPF. This discrepancy is most probably due to the increased number of exposed TiO_2 in latter compared to the former. The presence of pores would enhance the effective surface area and thus the number of exposed atoms, which capture chemisorbed water molecules. Another interesting observation that can be made from Table 1 is that the hydrophilicity is more retainable in TZPPF 24 h post UV-illumination. For TZP, the CA has increased to 32.73 from 25.27 (29.5% increase), whereas its value became 11.03 from 10.09 (9.3% increase) for TZPPF, which is comparatively much lower. Even 48 h after UV treatment, the CA of TZPPF has only reduced to 17.60 (74% deviation from the initial value), whereas that of TZP undergoes a change of 113% from its initial value. A behavior like this invokes curiosity and unraveling the reason behind it would be of great interest. Addition of ZrO_2 in TiO_2 is reported to generate more hydroxyl groups that can accept holes on UV radiation, thus preventing the electron−hole recombination leading to prolonged existence of hydrophilic nature in the sample.[14] However, this is not the only reason for a completely retainable hydrophilic nature observed in TZPPF, as such a nature is absent in TZP despite the presence of equal amount of ZrO_2.

The Raman imaging suggested that the pores in TZPPF have its upper walls made up of polymer (PMMA + PF127) and lower walls of TiO_2−ZrO_2. Because PMMA is hydrophobic, the upper walls would be hydrophobic, whereas the lower walls and base of the pores would be hydrophilic. The hydrophobic walls would roll off the dirt, which falls on the surface into the depths of the pores. However, chemisorbed water in the lower walls and base of the pores would prevent the dirt from coming into direct contact with them and getting attached. On the contrary, in TZP, the chances of chemisorptions are much lesser because of the reduced surface

DOI: 10.1021/acsomega.8b01940
ACS Omega 2018, 3, 14924−14932

area. Therefore, retainability of hydrophilic nature of TZPPF is much higher because of its porous structure.

For most applications such as photocatalytic devices and window panes, which require hydrophilic coatings, high transmittance in the visible region and high absorption in the UV region of the optical spectrum are a prerequisite. Most of the previously reported self-cleaning coatings with high transmittance have had very low thicknesses (in the nanometer range). However, for practical applications, coatings with such low thicknesses, whose production would need sophisticated and expensive techniques, are not desirable. Thick coatings with both hydrophilic nature and high transmittance on the other hand do not involve many complexities in their production and therefore are the need of the hour. In this study, it has already been discussed that both TZP and TZPPF show strong hydrophilic character after UV illumination at the same time having high thickness values (~2.7 μm). Figure 10

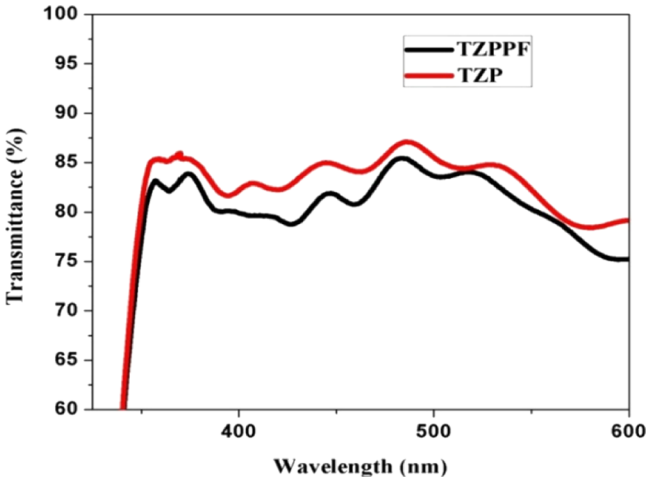

Figure 10. Comparative transmittance spectra of the films.

shows the transmission spectra of single- and double-templated thin films on the glass substrates. The TZPPF has a transmittance slightly lesser than that of TZP, even though their thicknesses values are really close. This discrepancy is due to the low transmittance of PF127 in the former. Still both films show high transmittance, and they are comparable to the results obtained for similar hydrophilic coatings with much lesser thickness values.[12,14,50] For TZPPF, the average transmittance in the visible region is 81%, whereas that for TZP is 84%. A sharp fall in the transmittance at 365 nm indicates the UV absorption by TiO_2 in the coatings. Thus, this study clearly indicates that the prepared samples are extremely potent candidates for self-cleaning applications.

CONCLUSIONS

The fact that the as-prepared TiO_2−ZrO_2−PMMA−PF127 hydrophilic coating is very thick and yet remains highly transparent in the UV−visible region makes it the first to be reported with a combination of favorable properties. The structure and surface studies have revealed that the chance of chemisorption is very high in the porous films as it can hold water for more time compared to a flat surface. The complicated surface of the porous film is created with polymer forming the outer walls of the pores, whereas TiO_2−ZrO_2 forming the inner walls and base. Whereas normal hydrophilic cleaning occurs in UV-irradiated non-porous coating, a complicated mechanism occurs in the porous one with a hydrophobic roll off of dirt into the pores followed by an easy washout with water.

EXPERIMENTAL SECTION

Materials and Reagents. Zirconium (IV) propoxide (ZP), titanium isopropoxide (TIP), and structure directing agent Pluronic F127 (PF127) were procured from Sigma-Aldrich, whereas PMMA with molecular weight 400 000 to 550 000 and diethanolamine (DEA) were purchased from Alfa Aesar and ethanol was obtained from Merck. All chemicals used were of analytical grade.

Precursor Solution for Dip Coating. Titania and zirconia sols were prepared separately by dissolving the corresponding precursors in ethanol. The typical weight percentage (wt %) of each component used was TIP/ZP/(PF127 + PMMA) = 70:25:5 wt %. Pluronic F127 and PMMA were dissolved in 3 mL of ethanol at 50 °C. Separately stirred inorganic precursor sols were mixed with polymer solution and stirred for about 2 h at 50 °C. Two or three drops of DEA, which acts as a chelating ligand, were added dropwise under vigorous stirring. On the contrary, single-templated TiO_2−ZrO_2 thin film prepared via the same method has 5 wt % of PMMA.

Both films were deposited on glass substrates by the dip-coating technique (withdrawal rate 2 mm/s) followed by aging for 10 days at 50 °C. Single- and double-templated samples are designated as TZP and TZPPF, respectively.

Dip-Coating Process. The dip-coating process was carried out using an ion exchanger dip-coating apparatus (Holmarc model no. HO-TH-IE01) to prepare thin films TZP and TZPPF.

UV Degradation Process. A UV degradation chamber built by Prism Foundation, Bangalore, composed of UV LED strips with a wavelength of 365 nm was used to study the UV degradation activity of the coated TZP and TZPPF thin films.

Characterization of Films. X-ray energy-dispersive spectrometry was conducted using Bruker model: XFlash 6/10. FTIR spectra of the samples were recorded on the transmittance mode using a PerkinElmer Spectrum 400 FTIR spectrometer in the range (400−4000) cm^{-1} with a resolution of 1 cm^{-1}. FESEM was performed on gold-coated samples using FEI model: Nova NanoSEM 450. The surface relief of the films was examined by AFM Nanoscope IIIa, Digital Instrument, USA, operating in the taping mode with a silicon tip. Surface hydrophilicity was studied from static WCA measurements using a SEO Phoenix CA analyser, and the images captured using a digital camera at room temperature. Measurements were done with deionized water, and volume of water drop was maintained at 6−8 μL using a microsyringe. The size and crystalline nature of colloidal TiO_2−ZrO_2 nanoparticles were investigated by TEM JEOL-JEM-2010, operating at an accelerating voltage of 200 kV. The 2D wide- and small-angle X-ray diffraction images were obtained using a XEUSS SAXS/WAXS system by Xenocs. The source for the radiation is Cu Kα with wavelength 1.54 Å. The images were converted into 1D pattern with the aid of Fit2D software. Raman spectra were recorded on a Horiba Jobin Yvon LabRAM-HR 800 spectrograph, equipped with a 632 nm helium−neon laser with 20 mW of power, attached to an Olympus BHX microscope. XPS was performed using a Kratos analytical X-ray photoelectron spectrometer.

DOI: 10.1021/acsomega.8b01940
ACS Omega 2018, 3, 14924−14932

AUTHOR INFORMATION

Corresponding Author

*E-mail: nvu100@gmail.com. Phone: +91 9745047850.

ORCID

N. V. Unnikrishnan: 0000-0001-5823-7199

Notes

The authors declare no competing financial interest.

ACKNOWLEDGMENTS

The present work was supported by DST-PURSE PII (SR. 417 & SR. 416 dated 27-2-2017). Also, we are thankful to Jacob K Chacko, Research Scholar, SB College, Changanacherry, Kerala, India, for his insightful discussions. G.G. thankfully acknowledges the financial support by UGC in the form of Dr. D. S. Kothari Post Doctoral Fellowship (no. F.4-2/2006(BSR)/CH/15-16/0211).

REFERENCES

(1) Parkin, I. P.; Palgrave, R. G. Self-cleaning coatings. *J. Mater. Chem.* **2005**, *15*, 1689−1695.

(2) Han, K.; Heng, L.; Jiang, L. Multiphase Media Antiadhesive Coatings: Hierarchical Self-Assembled Porous Materials Generated Using Breath Figure Patterns. *ACS Nano* **2016**, *10*, 11087−11095.

(3) Wenzel, R. N. Resistance of solid surfaces to wetting by water. *Ind. Eng. Chem.* **1936**, *28*, 988−994.

(4) Bormashenko, E. Progress in understanding wetting transitions on rough surfaces. *Adv. Colloid Interface Sci.* **2015**, *222*, 92−103.

(5) Bico, J.; Thiele, U.; Quéré, D. Wetting of textured surfaces. *Colloids Surf., A* **2002**, *206*, 41−46.

(6) Dong, Y.; Kong, J.; Phua, S. L.; Zhao, C.; Thomas, N. L.; Lu, X. Tailoring Surface Hydrophilicity of Porous Electrospun Nanofibers to Enhance Capillary and Push-Pull Effects for Moisture Wicking. *ACS Appl. Mater. Interfaces* **2014**, *6*, 14087−14095.

(7) Nakamura, C.; Manabe, K.; Tenjimbayashi, M.; Tokura, Y.; Kyung, K.-H.; Shiratori, S. Heat-Shielding and Self-Cleaning Smart Windows: Near-Infrared Reflective Photonic Crystals with Self-Healing Omniphobicity via Layer-by-Layer Self-Assembly. *ACS Appl. Mater. Interfaces* **2018**, *10*, 22731−22738.

(8) Shimomura, H.; Gemici, Z.; Cohen, R. E.; Rubner, M. F. Layer-by-Layer-Assembled High-Performance Broadband Antireflection Coatings. *ACS Appl. Mater. Interfaces* **2010**, *2*, 813−820.

(9) Reid, B.; Taylor, A.; Chen, Y.; Schmidt-Hansberg, B.; Guldin, S. Robust Operation of Mesoporous Antireflective Coatings under Variable Ambient Conditions. *ACS Appl. Mater. Interfaces* **2018**, *10*, 10315−10321.

(10) Kuo, C. Y.; Chen, Y. Y.; Lu, S. Y. A Facile Route To Create Surface Porous Polymer Films via Phase Separation for Antireflection Applications. *ACS Appl. Mater. Interfaces* **2009**, *1*, 72−75.

(11) Ren, T.; He, J. Substrate-Versatile Approach to Robust Antireflective and Superhydrophobic Coatings with Excellent Self-Cleaning Property in Varied Environments. *ACS Appl. Mater. Interfaces* **2017**, *9*, 34367−34376.

(12) Li, X.; He, J. Synthesis of Raspberry-Like SiO_2−TiO_2 Nanoparticles toward Antireflective and Self-Cleaning Coatings. *ACS Appl. Mater. Interfaces* **2013**, *5*, 5282−5290.

(13) Choi, J.; Ide, A.; Truong, Y. B.; Kyratzis, I. L.; Caruso, R. A. High surface area mesoporous titanium-zirconium oxide nanofibrous web: a heavy metal ion adsorbent. *J. Mater. Chem. A* **2013**, *1*, 5847−5853.

(14) Alotaibi, A. M.; Sathasivam, S.; Parkin, I. P. Aerosol assisted chemical vapour deposition of a ZrO_2−TiO_2 composite thin film with enhanced photocatalytic activity. *RSC Adv.* **2015**, *5*, 67944−67950.

(15) Zhang, J.; Li, L.; Liu, D.; Zhang, J.; Hao, Y.; Zhang, W. Multi-layer and open three-dimensionally ordered macroporous TiO_2−ZrO_2 composite: diversified design and the comparison of multiple mode photocatalytic performance. *Mater. Des.* **2015**, *86*, 818−828.

(16) Fateh, R.; Dillert, R.; Bahnemann, D. Preparation and Characterization of Transparent Hydrophilic Photocatalytic TiO_2/SiO_2 Thin Films on Polycarbonate. *Langmuir* **2013**, *29*, 3730−3739.

(17) Xi, B.; Verma, L. K.; Li, J.; Bhatia, C. S.; Danner, A. J.; Yang, H.; Zeng, H. C. TiO_2 Thin Films Prepared via Adsorptive Self-Assembly for Self-Cleaning Applications. *ACS Appl. Mater. Interfaces* **2012**, *4*, 1093−1102.

(18) Hussein, A. M.; Shende, R. V. Enhanced hydrogen generation using ZrO_2-modified coupled ZnO/TiO_2nanocomposites in the absence of noble metal co-catalyst. *Int. J. Hydrogen Energy* **2014**, *39*, 5557−5568.

(19) Shao, G. N.; Imran, S. M.; Jeon, S. J.; Engole, M.; Abbas, N.; Haider, M. S.; Kang, S. J.; Kim, H. T. Sol-gel synthesis of photoactive zirconia-titania from metal salts and investigation of their photocatalytic properties in the photodegradation of methylene blue. *Powder Technol.* **2014**, *258*, 99−109.

(20) Fukumoto, T.; Yoshioka, T.; Nagasawa, H.; Kanezashi, M.; Tsuru, T. Development and gas permeation properties of microporous amorphous TiO_2−ZrO_2−organic composite membranes using chelating ligands. *J. Membr. Sci.* **2014**, *461*, 96−105.

(21) Goswami, P.; Ganguli, J. N. Tuning the band gap of mesoporous Zr-doped TiO_2 for effective degradation of pesticide quinalphos. *Dalton Trans.* **2013**, *42*, 14480−14490.

(22) Prakashan, V. P.; Sajna, M. S.; Gejo, G.; Sanu, M. S.; Biju, P. R.; Cyriac, J.; Unnikrishnan, N. V. Perceiving impressive optical properties of ternary SiO_2-TiO_2-ZrO_2:Eu^{3+} solgel glasses with high reluctance for concentration quenching: An experimental approach. *J. Non-Cryst. Solids* **2018**, *482*, 116−125.

(23) Zhou, Q.; Zhang, Z.; Chen, T.; Guo, X.; Zhou, S. Preparation and characterization of thermosensitive pluronic F127-b-poly(ε-caprolactone) mixed micelles. *Colloids Surf., B* **2011**, *86*, 45−57.

(24) Naumenko, A.; Gnatiuk, I.; Smirnova, N.; Eremenko, A. Characterization of sol−gel derived TiO_2/ZrO_2 films and powders by Raman spectroscopy. *Thin Solid Films* **2012**, *520*, 4541−4546.

(25) Su, W.; Zhang, J.; Feng, Z.; Chen, T.; Ying, P.; Li, C. Surface Phases of TiO_2 Nanoparticles Studied by UV Raman Spectroscopy and FT-IR Spectroscopy. *J. Phys. Chem. C* **2008**, *112*, 7710−7716.

(26) Livraghi, S.; Olivero, F.; Paganini, M. C.; Giamello, E. Titanium Ions Dispersed into the ZrO2 Matrix: Spectroscopic Properties and Photoinduced Electron Transfer. *J. Phys. Chem. C* **2010**, *114*, 18553−18558.

(27) Miller, J. M.; Lakshmi, L. J. Spectroscopic Characterization of Sol-Gel-Derived Mixed Oxides. *J. Phys. Chem. B* **1998**, *102*, 6465−6470.

(28) Colomer, M. T.; Maczka, M. Mixed conductivity, structural and microstructural characterization of titania-doped yttria tetragonal zirconia polycrystalline/titania-doped yttria stabilized zirconia composite anode matrices. *J. Solid State Chem.* **2011**, *184*, 365−372.

(29) Fan, M.; Hu, S.; Ren, B.; Wang, J.; Jing, X. Synthesis of nanocomposite TiO_2/ZrO_2 prepared by different templates and photocatalytic properties for the photodegradation of Rhodamine B. *Powder Technol.* **2013**, *235*, 27−32.

(30) Charanpahari, A.; Ghugal, S. G.; Umare, S. S.; Sasikala, R. Mineralization of malachite green dye over visible light responsive bismuth doped TiO_2−ZrO_2 ferromagnetic nanocomposites. *New J. Chem.* **2015**, *39*, 3629−3638.

(31) Grosso, D.; Soler-Illia, G. J. d. A. A.; Crepaldi, E. L.; Cagnol, F.; Sinturel, C.; Bourgeois, A.; Brunet-Bruneau, A.; Amenitsch, H.; Albouy, P. A.; Sanchez, C. Highly Porous TiO_2 Anatase Optical Thin Films with Cubic Mesostructure Stabilized at 700 °C. *Chem. Mater.* **2003**, *15*, 4562−4570.

(32) Mountjoy, G.; Holland, M. A.; Wallidge, G. W.; Gunawidjaja, P.; Smith, M. E.; Pickup, D. M.; Newport, R. J. Structural Characterization of Mixed $(TiO_2)_x(ZrO_2)_y(SiO_2)_{1-x-y}$ Sol-Gels ($0.05 \leq x, y \leq 0.15$) by a Combination of X-ray and Spectroscopy Techniques. *J. Phys. Chem. B* **2003**, *107*, 7557−7566.

(33) Smarsly, B.; Grosso, D.; Brezesinski, T.; Pinna, N.; Boissière, C.; Antonietti, M.; Sanchez, C. Highly Crystalline Cubic Mesoporous

DOI: 10.1021/acsomega.8b01940
ACS Omega 2018, 3, 14924−14932

TiO_2 with 10-nm Pore Diameter Made with a New Block Copolymer Template. *Chem. Mater.* **2004**, *16*, 2948−2952.
(34) Zhang, Y.; Li, J.; Wang, J. Substrate-Assisted Crystallization and Photocatalytic Properties of Mesoporous TiO_2 Thin Films. *Chem. Mater.* **2006**, *18*, 2917−2923.
(35) Wong, M. S.; Jeng, E. S.; Ying, J. Y. Supramolecular Templating of Thermally Stable Crystalline Mesoporous Metal Oxides Using Nanoparticulate Precursors. *Nano Lett.* **2001**, *1*, 637−642.
(36) Brezesinski, T.; Fischer, A.; Iimura, K.; Sanchez, C.; Grosso, D.; Antonietti, M.; Smarsly, B. M. Generation of Self-Assembled 3D Mesostructured SnO_2 Thin Films with Highly Crystalline Frameworks. *Adv. Funct. Mater.* **2006**, *16*, 1433−1440.
(37) Lekshmy, S. S.; Joy, K. Structural and optoelectronic properties of indium doped SnO_2 thin films deposited by sol gel technique. *J. Mater. Sci.: Mater. Electron.* **2014**, *25*, 1664−1672.
(38) Berlin, I. J.; Lakshmi, J. S.; Lekshmy, S. S.; Daniel, G. P.; Thomas, P. V.; Joy, K. Effect of sol temperature on the structure, morphology, optical and photoluminescence properties of nanocrystalline zirconia thin films. *J. Sol-Gel Sci. Technol.* **2011**, *58*, 669−676.
(39) Xin, B.; Hao, J. Reversibly switchable wettability. *Chem. Soc. Rev.* **2010**, *39*, 769−782.
(40) Kamegawa, T.; Shimizu, Y.; Yamashita, H. Superhydrophobic Surfaces with Photocatalytic Self- Cleaning Properties by Nanocomposite Coating of TiO_2 and Polytetrafluoroethylene. *Adv. Mater.* **2012**, *24*, 3697−3700.
(41) Lin, X.; Lu, F.; Chen, Y.; Liu, N.; Cao, Y.; Xu, L.; Zhang, W.; Feng, L. Electricity-induced switchable wettability and controllable water permeation based on 3D copper foam. *Chem. Commun.* **2015**, *51*, 16237−16240.
(42) Abraham, R.; Varughese, K. T.; Isac, J.; Thomas, S. Wetting Properties of Barium Sodium Niobate Filled Polystyrene Nanocomposite. *Macromol. Symp.* **2012**, *315*, 1−14.
(43) Sakai, N.; Wang, R.; Fujishima, A.; Watanabe, T.; Hashimoto, K. Effect of Ultrasonic Treatment on Highly Hydrophilic TiO_2 Surfaces. *Langmuir* **1998**, *14*, 5918−5920.
(44) Yang, T.S.; Shiu, C.B.; Wong, M.S. Structure and hydrophilicity of titanium oxide films prepared by electron beam evaporation. *Surf. Sci.* **2004**, *548*, 75−82.
(45) Bharti, B.; Kumar, S.; Lee, H.-N.; Kumar, R. Formation of oxygen vacancies and Ti^{3+} state in TiO_2 thin film and enhanced optical properties by air plasma treatment. *Sci. Rep.* **2016**, *6*, 32355.
(46) Rtimi, S.; Pulgarin, C.; Sanjines, R.; Nadtochenko, V.; Lavanchy, J.C.; Kiwi, J. Preparation and Mechanism of Cu-Decorated TiO_2−ZrO_2 Films Showing Accelerated Bacterial Inactivation. *ACS Appl. Mater. Interfaces* **2015**, *7*, 12832−12839.
(47) Liu, C.; Yang, D.; Jiao, Y.; Tian, Y.; Wang, Y.; Jiang, Z. Biomimetic Synthesis of TiO_2−SiO_2−Ag Nanocomposites with Enhanced Visible-Light Photocatalytic Activity. *ACS Appl. Mater. Interfaces* **2013**, *5*, 3824−3832.
(48) Takeuchi, M.; Sakamoto, K.; Martra, G.; Coluccia, S.; Anpo, M. Mechanism of Photoinduced Superhydrophilicity on the TiO_2 Photocatalyst Surface. *J. Phys. Chem. B* **2005**, *109*, 15422−15428.
(49) Atuchin, V. V.; Kesler, V. G.; Pervukhina, N. V.; Zhang, Z. Ti 2p and O 1s core levels and chemical bonding in titanium-bearing oxides. *J. Electron Spectrosc. Relat. Phenom.* **2006**, *152*, 18−24.
(50) Prado, R.; Beobide, G.; Marcaide, A.; Goikoetxea, J.; Aranzabe, A. Development of multifunctional sol-gel coatings: Anti-reflection coatings with enhanced self-cleaning capacity. *Sol. Energy Mater. Sol. Cells* **2010**, *94*, 1081−1088.

DOI: 10.1021/acsomega.8b01940
ACS Omega 2018, 3, 14924−14932